Gravity currents under oscillatory forcing

Cem Bingol[1], Matias Duran-Matute[1], Rui Zhu[2,3] Eckart Meiburg[3], and Herman J. H. Clercx[1]†

[1]Fluids and Flows group and J.M. Burgers Center for Fluid Dynamics, Department of Applied Physics, Eindhoven University of Technology, P.O. Box 513, 5600 MB Eindhoven, The Netherlands

[2]Ocean College, Zhejiang University, Zhoushan 316021, PR China

[3]Department of Mechanical Engineering, University of California at Santa Barbara, Santa Barbara, CA 93106, USA

1. Movie

The Supplementary Material contains three movies (in separate files). Movie 1 shows the evolution of the gravity current with $KC_b = 50$ and $Fr = 1$ for $50 \leqslant t \leqslant 200$ complementing figure 4. Movie 2 provides a comparison of the density field evolution for the freely-evolving gravity current and those with $KC_b = 5$, 10, 25, 50 and 100. These animations cover the evolution between $t = 0$ and $t = 200$. Finally, movie 3 shows the evolution of the gravity current with $KC_b = 50$ and $Fr = 0$, 0.25, 0.5, 1 and 2 for $50 \leqslant t \leqslant 200$.

2. Other supplementary material

Other supplementary material contains complementary snapshots of the density field taken at $t = 200$, 300 and 400. The general characteristics of the density redistribution processes in the gravity current in the presence of oscillatory forcing is shown in figure 4 in Section 4.1. Here, we display the density field plots for different phases for simulations with $KC_b = 50$ and $Fr = 1$ for simulations ending at $t = 200$, 300, and 400 (figures S1 - S3).

Similarly, in Section 4.2, we demonstrated the density fields at $\phi = 90°$ (figure 5) for oscillations concluding at $t = 100$. Here, we are displaying density fields at $\phi = 90°$ for oscillations ending at $t = 200$, 300, and 400 (figures S4 - S6). In Section 4.2, we also showed the density fields of the zoomed front of the gravity current for oscillations ending at $t = 100$. Here, we are also including the density fields of the zoomed front at $\phi = 90°$ for $t = 200$, 300, and 400, see figures S7 - S9.

In Section 4.3, we have shown the density redistribution process in the gravity current in the second half of the oscillation cycle at $\phi = 360°$ where it was coinciding with $t = 100$ for simulations with different KC_b values (figure 7). Here, we follow the same approach and display the density fields at $\phi = 360°$ for $t = 200$, 300, and 400 (figures S10 - S12).

Lastly, in Section 6.2 we briefly discuss a different cross-section of the $Fr - KC_b$ parameter space. We show some of the results in figures S13 - S16 (equivalents of figures 5, 7, 10 and 11).

† Email address for correspondence: h.j.h.clercx@tue.nl

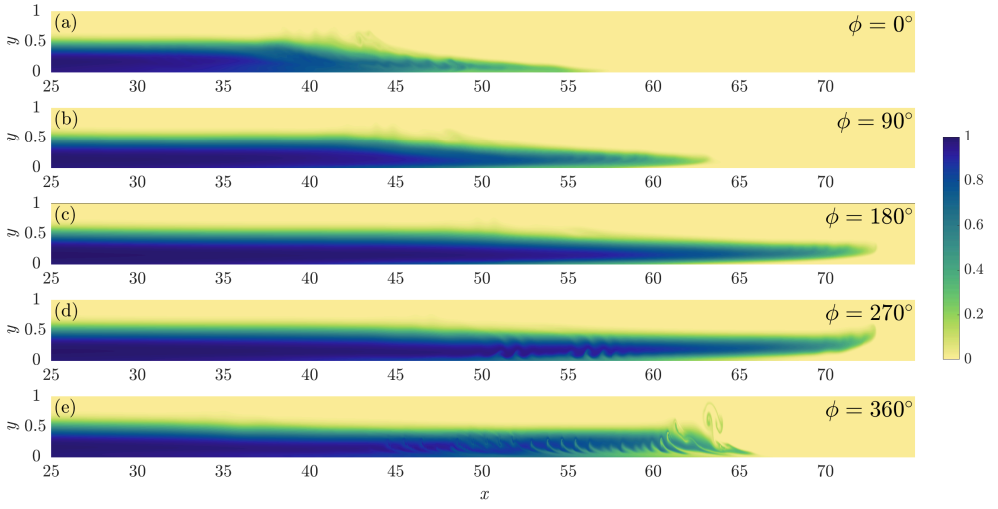

FIGURE S1. Dimensionless density fields for $KC_b = 50$ at different phases of the imposed ambient flow ($L_{AR} \approx 3.3$): (a) $\phi = 0°$ at $t = 150$, (b) $\phi = 90°$ at $t = 162.5$, (c) $\phi = 180°$ at $t = 175$, (d) $\phi = 270°$ at $t = 187.5$, and (e) $\phi = 360°$ at $t = 200$. The value of the density (with $0 \leqslant \rho \leqslant 1$) is indicated by the color bar.

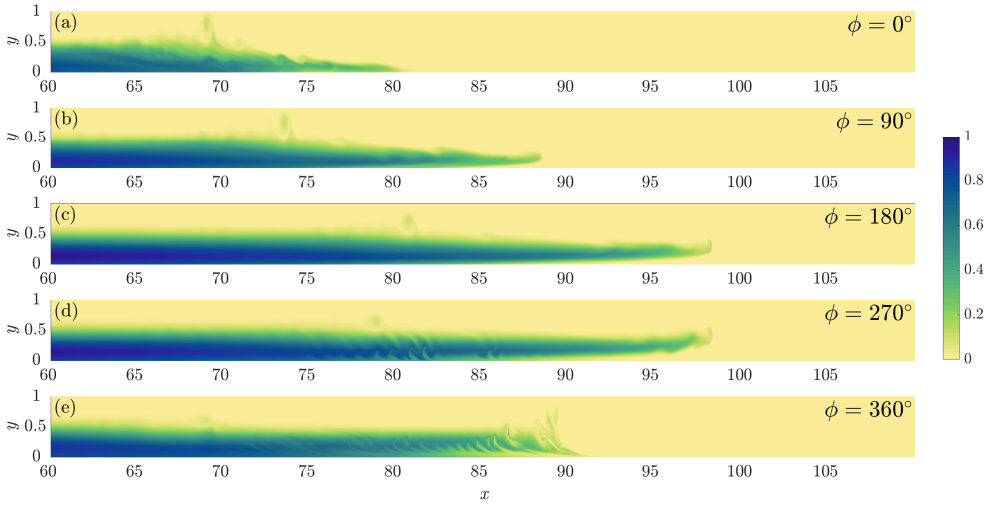

FIGURE S2. As in figure S1 with (a) $\phi = 0°$ at $t = 250$, (b) $\phi = 90°$ at $t = 262.5$, (c) $\phi = 180°$ at $t = 275$, (d) $\phi = 270°$ at $t = 287.5$, and (e) $\phi = 360°$ at $t = 300$.

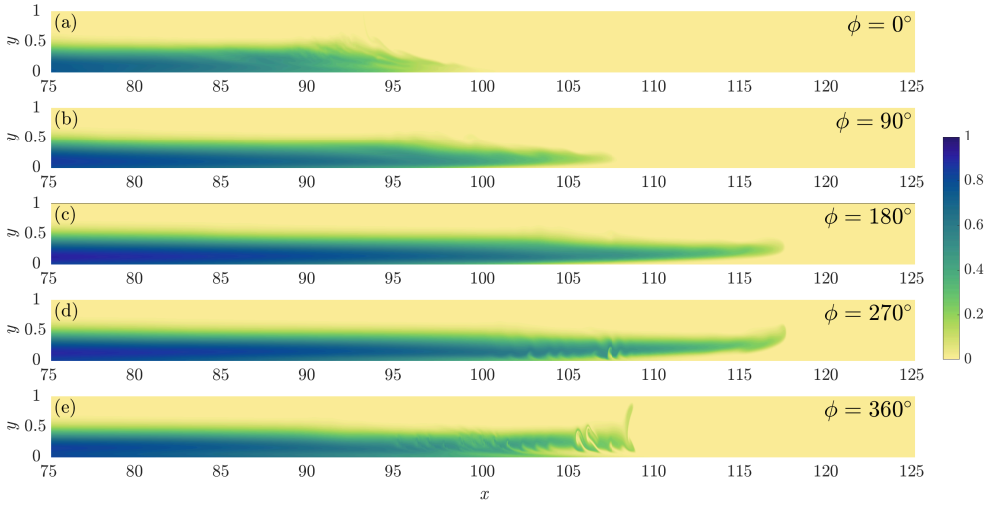

FIGURE S3. As in figure S1 with (a) $\phi = 0°$ at $t = 350$, (b) $\phi = 90°$ at $t = 362.5$, (c) $\phi = 180°$ at $t = 375$, (d) $\phi = 370°$ at $t = 387.5$, and (e) $\phi = 360°$ at $t = 400$.

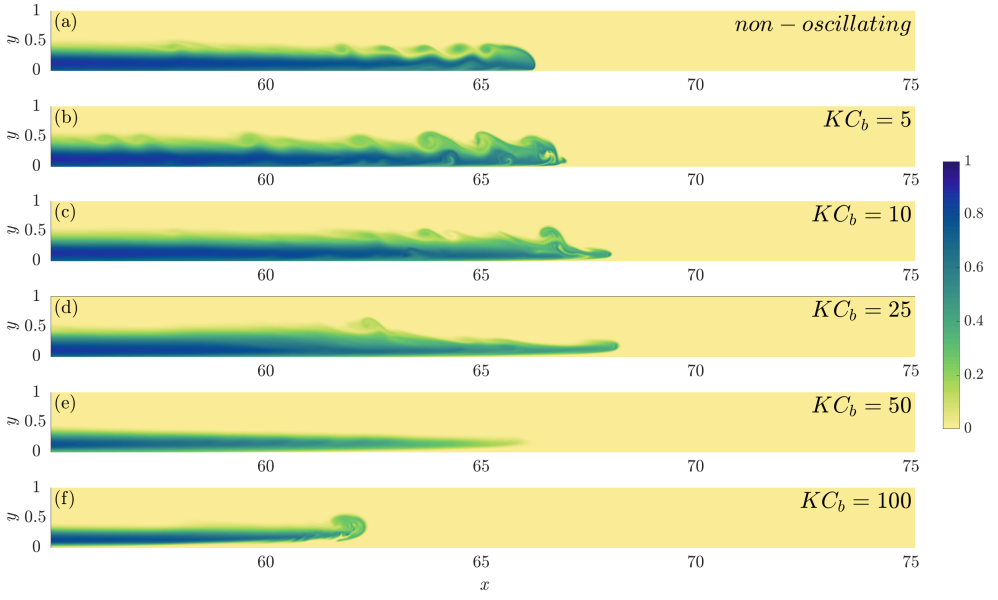

FIGURE S4. Dimensionless density fields ($L_{AR} \approx 1.4$) for the non-oscillating case, panel (a), and those for different KC_b, panels (b)-(f). For the oscillating cases they are all obtained at the same phase of the forcing cycle, $\phi = 90°$. The time instance for the snapshots of the density fields are: (a) $t = 196.25$, (b) $t = 196.25$ ($KC_b = 5$), (c) $t = 192.5$ ($KC_b = 10$), (d) $t = 181.25$ ($KC_b = 25$), (e) $t = 162.5$ ($KC_b = 50$), and (f) $t = 125$ ($KC_b = 100$). The value of the density (with $0 \leqslant \rho \leqslant 1$) is indicated by the color bar.

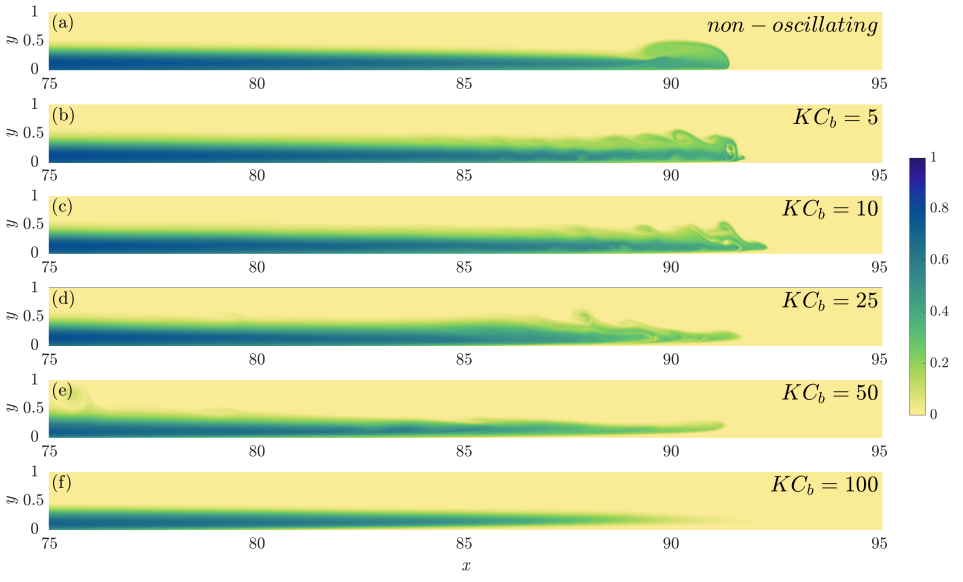

FIGURE S5. As in Fig S4. The time instance for the snapshots of the density fields are: (a) $t = 296.25$, (b) $t = 296.25$ ($KC_b = 5$), (c) $t = 292.5$ ($KC_b = 10$), (d) $t = 281.25$ ($KC_b = 25$), (e) $t = 262.5$ ($KC_b = 50$), and (f) $t = 225$ ($KC_b = 100$).

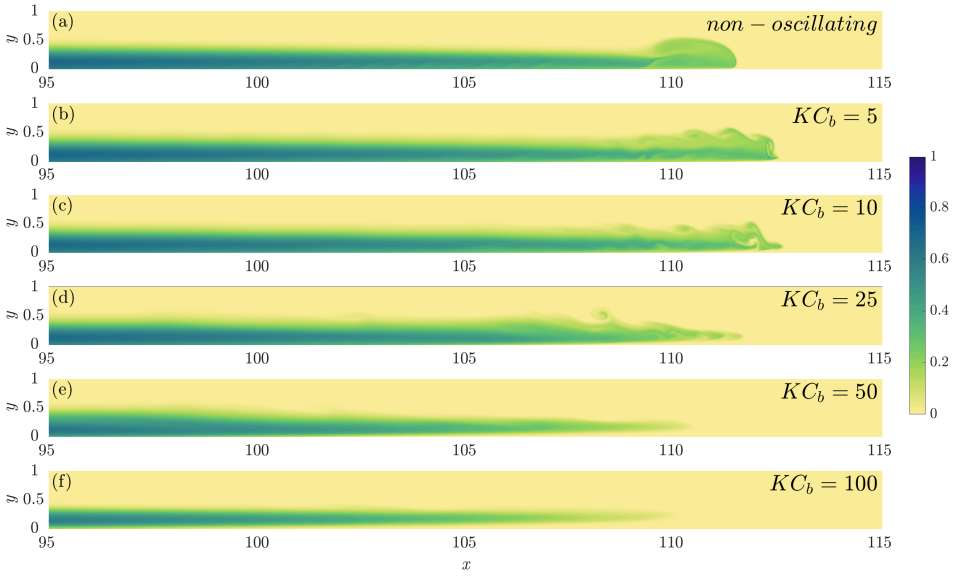

FIGURE S6. As in Fig S4. The time instance for the snapshots of the density fields are: (a) $t = 396.25$, (b) $t = 396.25$ ($KC_b = 5$), (c) $t = 392.5$ ($KC_b = 10$), (d) $t = 381.25$ ($KC_b = 25$), (e) $t = 362.5$ ($KC_b = 50$), and (f) $t = 325$ ($KC_b = 100$).

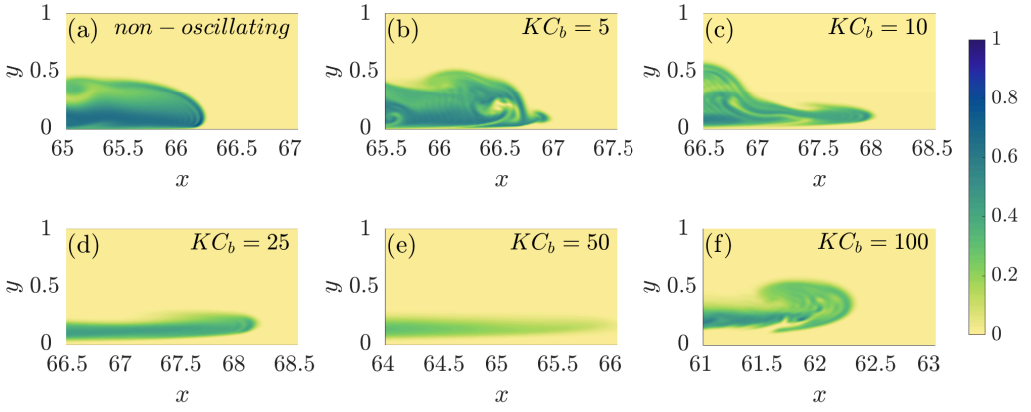

FIGURE S7. Dimensionless density fields for the non-oscillating case, panel (a), and those for different KC_b, panels (b)-(f) zoomed in at the front of gravity current ($L_{AR} = 1$). For the oscillating cases they are all obtained at the same phase of the forcing cycle, $\phi = 90^\circ$. The time instance for the snapshots of the density fields are: (a) $t = 196.25$, (b) $t = 196.25$ ($KC_b = 5$), (c) $t = 192.5$ ($KC_b = 10$), (d) $t = 181.25$ ($KC_b = 25$), (e) $t = 162.5$ ($KC_b = 50$), and (f) $t = 125$ ($KC_b = 100$). The value of the density (with $0 \leqslant \rho \leqslant 1$) is indicated by the color bar.

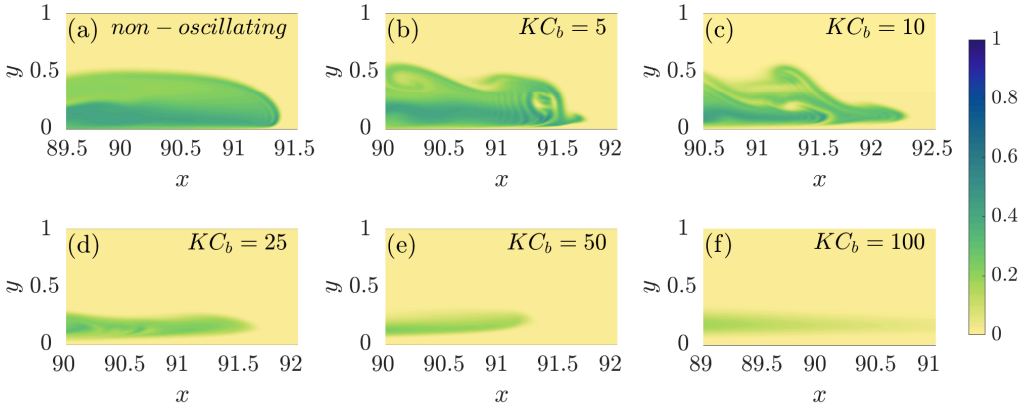

FIGURE S8. As in Fig S7. The time instance for the snapshots of the density fields are: (a) $t = 296.25$, (b) $t = 296.25$ ($KC_b = 5$), (c) $t = 292.5$ ($KC_b = 10$), (d) $t = 281.25$ ($KC_b = 25$), (e) $t = 262.5$ ($KC_b = 50$), and (f) $t = 225$ ($KC_b = 100$).

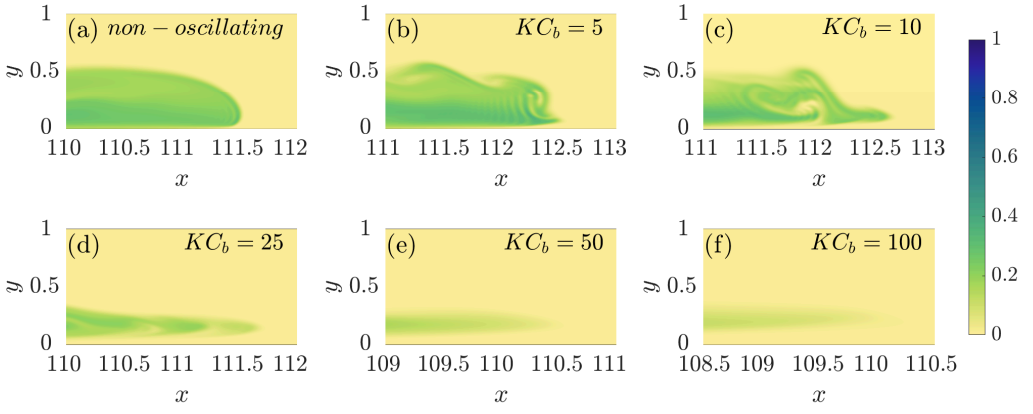

FIGURE S9. As in Fig S7. The time instance for the snapshots of the density fields are: (a) $t = 396.25$, (b) $t = 396.25$ ($KC_b = 5$), (c) $t = 392.5$ ($KC_b = 10$), (d) $t = 381.25$ ($KC_b = 25$), (e) $t = 362.5$ ($KC_b = 50$), and (f) $t = 325$ ($KC_b = 100$).

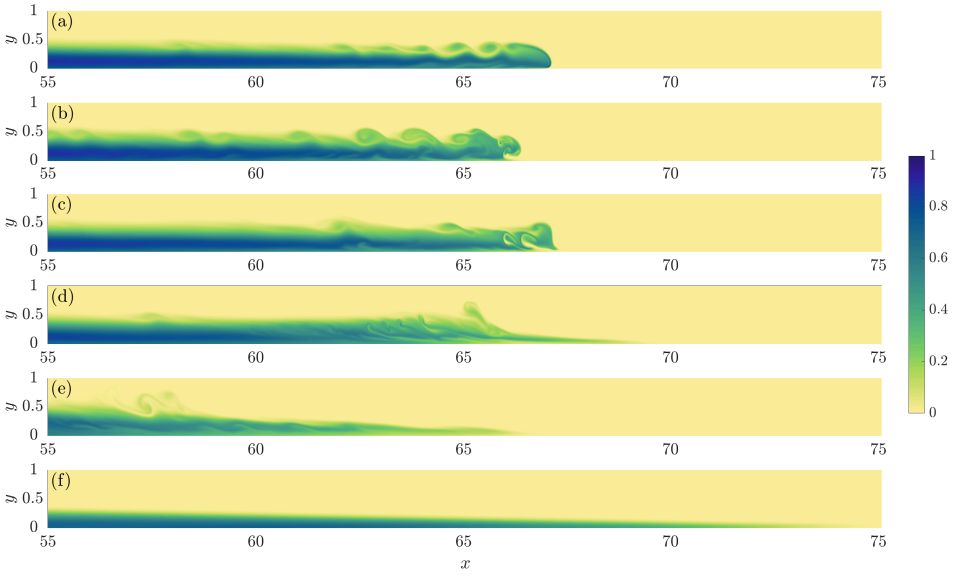

FIGURE S10. Dimensionless density fields at $t = 200$ which coincides with $\phi = 360^\circ$ for cases with different period of oscillations ($L_{AR} \approx 1.4$). (a) Non-oscillating case, (b) $KC_b = 5$, (c) $KC_b = 10$, (d) $KC_b = 25$, (e) $KC_b = 50$, (f) $KC_b = 100$. The value of the density (with $0 \leqslant \rho \leqslant 1$) is indicated by the color bar.

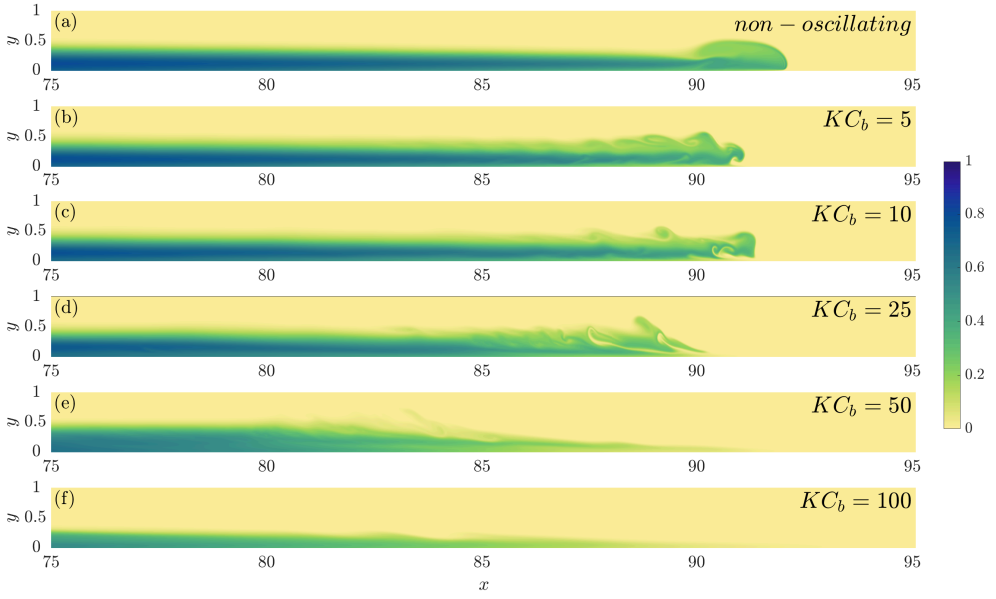

FIGURE S11. As in Fig S10 but at $t = 300$.

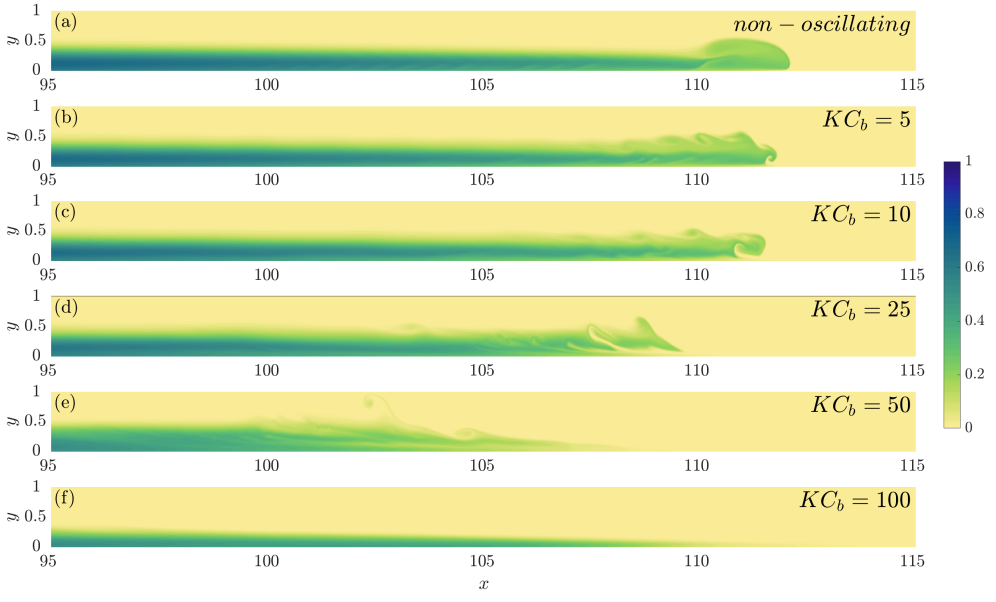

FIGURE S12. As in Fig S10 but at $t = 400$.

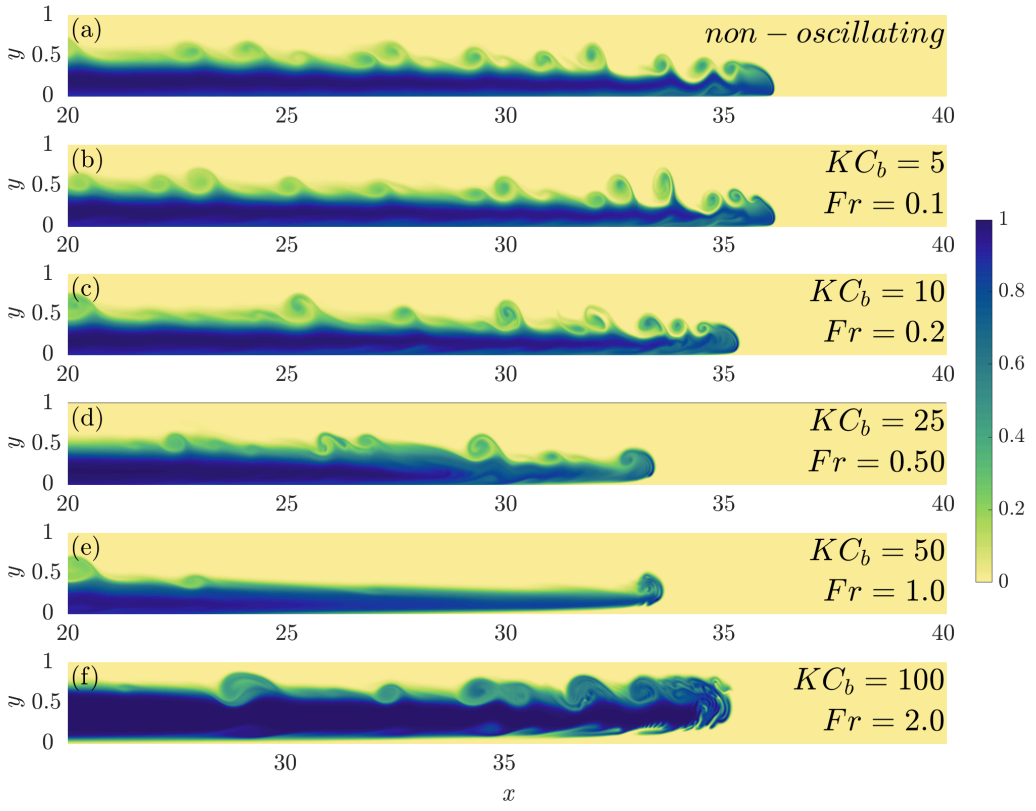

FIGURE S13. Dimensionless density fields (with $L_{AR} \approx 1.8$) for the non-oscillating case, panel (a), and those for different KC_b and $Fr = 1$, but with $Fr/KC_b = 0.02$), panels (b)-(f). For the oscillating cases they are all obtained at the same phase of the forcing cycle, $\phi = 90°$. The time instance for the snapshots of the density fields are: (a) $t = 96.25$, (b) $t = 96.25$ (gone through 19.25 oscillation cycles; $KC_b = 5$), (c) $t = 92.5$ (9.25 cycles; $KC_b = 10$), (d) $t = 81.25$ (3.25 cycles; $KC_b = 25$), (e) $t = 62.5$ (1.25 cycle; $KC_b = 50$), and (f) $t = 25$ (0.25 cycle; $KC_b = 100$). For panel (f) we plot the density field for $25 \leqslant x \leqslant 45$ since the front of the gravity current is located at $x \approx 40$. The value of the density (with $0 \leqslant \rho \leqslant 1$) is indicated by the color bar.

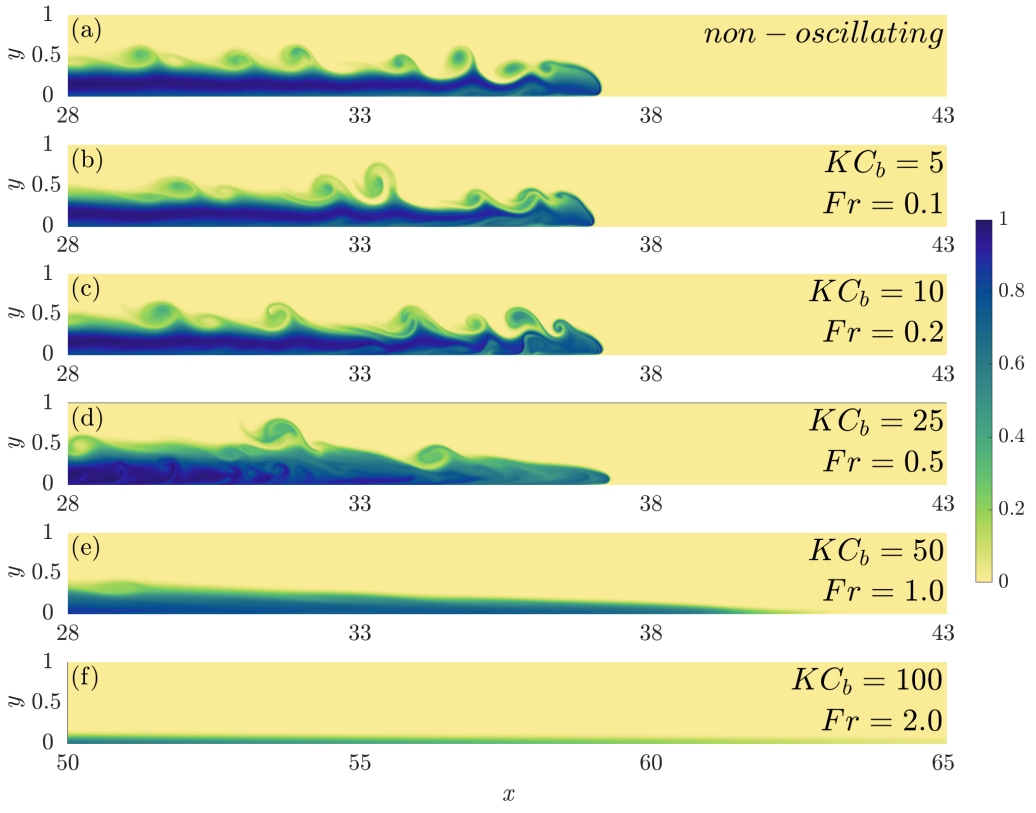

FIGURE S14. Dimensionless density fields (with $L_{AR} \approx 1.3$) for the non-oscillating case, panel (a), and those for different KC_b and $Fr = 1$, but with $Fr/KC_b = 0.02$), panels (b)-(f). They are all shown for $t = 100$, which coincides with $\phi = 360°$ for the oscillating cases. For panel (f) we plot the density field for $50 \leqslant x \leqslant 65$ since the front of the gravity current (although not very well defined) is located near $x \approx 65$. The value of the density (with $0 \leqslant \rho \leqslant 1$) is indicated by the color bar.

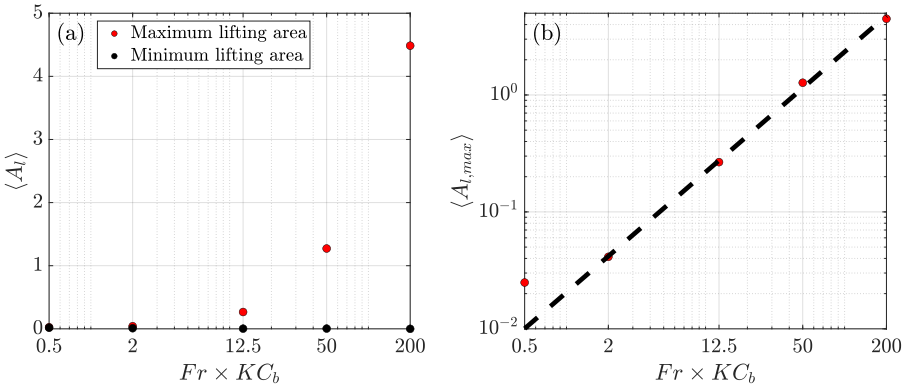

FIGURE S15. (a) The average maximum lifting area $\langle A_{l,max} \rangle$ (red symbols) and average minimum lifting area $\langle A_{l,min} \rangle$ (black symbols) as function of $FrKC_b$. For all cases, $Fr/KC_b = 0.02$ (based on the combinations shown in figures S13 and S14). (b) Scaling of the average maximum lifting area $\langle A_{l,max} \rangle$; the black dashed line indicates a scaling $\langle A_{l,max} \rangle \propto (FrKC_b)^{1.0}$. The fit is based on nonlinear least squares from the data $FrKC_b \in$(2, 12.5, 50, 200).

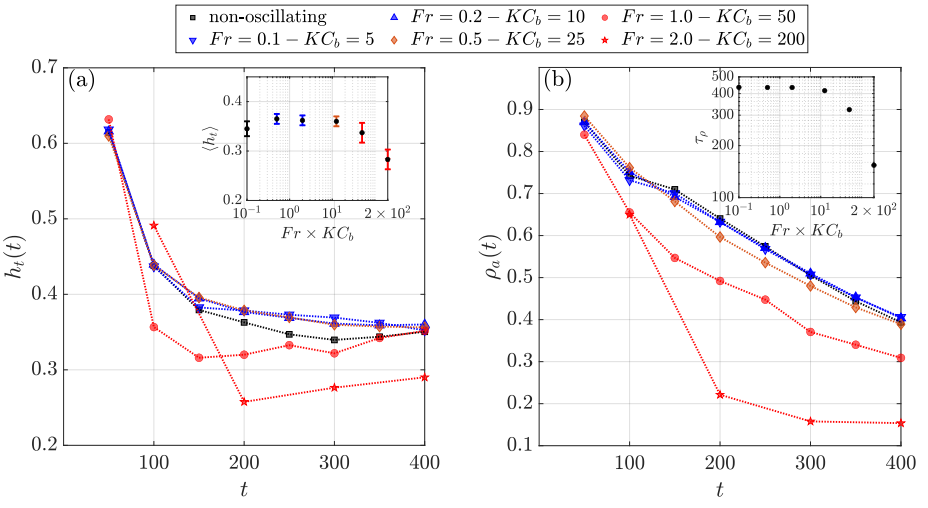

FIGURE S16. (a) The average current thickness $h_t(t)$ of the gravity current front, and (b) the average density $\rho_a(t)$ in the gravity current front for the freely-evolving gravity current and the five cases with an externally-applied oscillating pressure gradient. For all cases, $Fr/KC_b = 0.02$ (based on the combinations shown in figures S13 and S14). The horizontal extent of the gravity current front is taken as $\Delta L = 15$. The inset in (a) shows the current thickness averaged over the times 200, 250, ..., 400. Estimated error margins are included. The inset in (b) shows the density relaxation time τ_ρ for the same cases. For both insets, the values for the freely-evolving case are on the vertical axis.